

# 3D Registration for Self-Occluded Objects in Context

Zheng Dang  
Xi'an Jiaotong University  
dangzheng713@stu.xjtu.edu.cn

Fei Wang  
Xi'an Jiaotong University  
wfx@mail.xjtu.edu.cn

Mathieu Salzmann  
EPFL-CVLab & ClearSpace  
mathieu.salzmann@epfl.ch

## Abstract

While much progress has been made on the task of 3D point cloud registration, there still exists no learning-based method able to estimate the 6D pose of an object observed by a 2.5D sensor in a scene. The challenges of this scenario include the fact that most measurements are outliers depicting the object's surrounding context, and the mismatch between the complete 3D object model and its self-occluded observations. We introduce the first deep learning framework capable of effectively handling this scenario. Our method consists of an instance segmentation module followed by a pose estimation one. It allows us to perform 3D registration in a one-shot manner, without requiring an expensive iterative procedure. We further develop an on-the-fly rendering-based training strategy that is both time- and memory-efficient. Our experiments evidence the superiority of our approach over the state-of-the-art traditional and learning-based 3D registration methods.

## 1. Introduction

3D registration aims to determine the rigid transformation, i.e., 3D rotation and 3D translation, between two 3D point sets. The traditional approach to this problem is the Iterative Closest Point (ICP) algorithm [4]. In its vanilla version, this iterative algorithm easily gets trapped in poor local optima. While globally-optimal solutions [44, 49] have been proposed to remedy this, they lack robustness to noise, thus greatly reducing their practical applicability.

Recently, learning-based methods [1, 38] were shown to outperform the previous traditional, optimization-based techniques. While these initial methods were designed to work under the unrealistic assumption that both point sets are fully observed, even at test time, follow-up works focused on the more practical partial-to-partial registration scenario [39, 45]. Nevertheless, these techniques still assume the observations to depict a point-cloud in full 3D. In practice, however, many sensors, such as depth cameras and LiDARs, only provide 2.5D measurements. Furthermore, when focusing on objects, as we do, and not entire scenes, as in, e.g., [7], one needs to handle the measurements com-

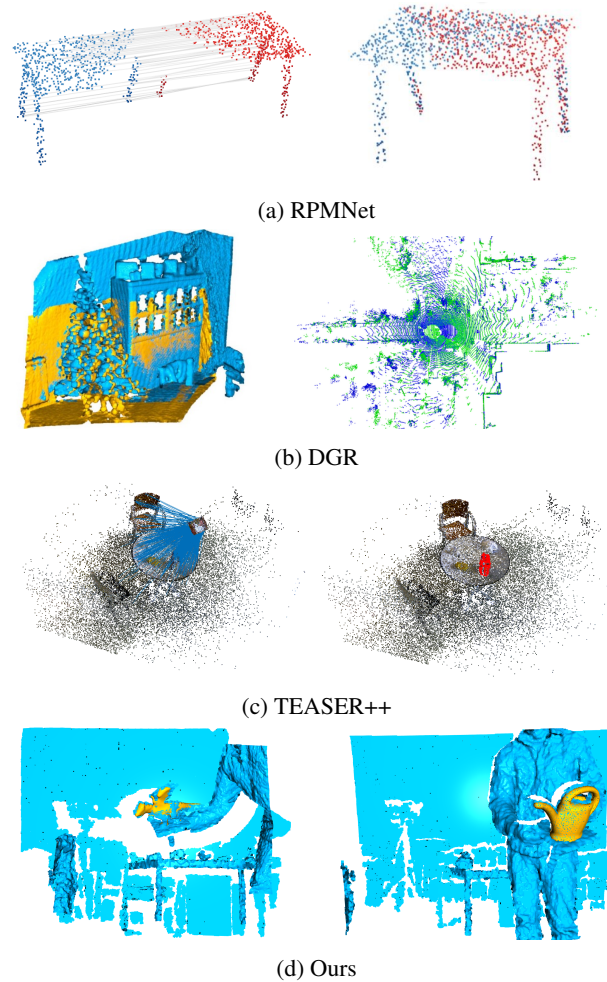


Figure 1: In contrast to object-to-object registration, as done by, e.g., RPMNet [45], and scene-to-scene registration, as performed by, e.g., DGR [7], we tackle the challenging task of estimating the 6D pose of an object in a scene captured with a 2.5D sensor. While TEASER++ [43] showcased this for the case where the object model is in one-to-one correspondence with the observed point set, we propose a learning-based approach able to handle the scenario where the model is self-occluded. (RPMNet, DGR and TEASER++ were borrowed from the original papers.)

ing from the object’s context, i.e., the scene itself, which are irrelevant to estimate the object 6D pose but are nonetheless captured by the sensor.

Only few methods have attempted to estimate the 6D pose of an object in a scene from depth data [36, 42, 43]. To this end, these methods extract handcrafted representations of the 3D points, such as Point Pair Features (PPF) [36] or Fast Point Feature Histograms (FPFH) [42, 43] and handle the presence of contextual information by casting the problem as an outlier removal task. As such, they do not truly focus on the 2.5D nature of the measurements, and, for example, the effectiveness of the most recent one, TEASER++ [43], was only demonstrated in a restricted scenario, where the reference object point-cloud was in one-to-one correspondence with that observed in the scene context. Furthermore, these methods all rely on handcrafted features, and, to the best of our knowledge, 6D pose estimation of a self-occluded object in context, as illustrated by Fig. 1, has never been tackled in a deep learning fashion.

In this paper, we address this by introducing a deep learning framework for 3D registration of self-occluded objects in context. Our approach consists of an instance segmentation module to separate the object from the surrounding scene, followed by a 6D pose estimation module able to handle the mismatch between the complete 3D model and the observed, self-occluded point-set. Our method works in a one-shot fashion; at test time, we estimate the object pose by a single forward pass through the network, without the need for an expensive iterative procedure. This makes our approach amenable to practical applications relying on 2.5D sensors and requiring real-time performance, such as autonomous navigation and robotics manipulation.

Our contributions can be summarized as follows:

- We tackle, for the first time, the challenging problem of estimating the 6D pose of a self-occluded object in context in a learning-based manner.
- We develop a one-shot framework to address this task, consisting of an instance segmentation and a pose estimation module.
- We design a memory- and computation-effective training method based on on-the-fly rendering, which prevents the need for expensive offline rendering and storing of the generated data, as required by standard procedures, such as BlenderProc [11], while giving us access to virtually infinite amounts of training data.

We demonstrate the effectiveness of our approach using the ModelNet40 benchmark, from which we generate depth maps to match our application scenario. Our approach significantly outperforms the state-of-the-art traditional and learning-based registration techniques [38, 39], including our main competitor TEASER++ [42, 43]. We will make our code publicly available.

## 2. Related Work

**Traditional point cloud registration.** ICP is the best-known algorithm for solving the point cloud registration problem. It comprises two steps: One whose goal is to find the closest target point for each source point to generate 3D-3D correspondences, and the other that computes the rigid transformation from these correspondences by solving a least-square problem. These two steps are repeated until a termination condition is satisfied. Several variants, such as Generalized-ICP [34] and Sparse ICP [6], have been proposed to improve robustness to noise and mismatches, and we refer the reader to [24, 29] for a complete review of ICP-based strategies. The main drawback of these methods is their requirement for a reasonable initialization to converge to a good solution. Only relatively recently has this weakness been addressed by the globally-optimal registration method Go-ICP [44]. In essence, this approach follows a branch-and-bound strategy to search the entire 3D motion space  $SE(3)$ . Motivated by this, other approaches to finding a global solution have been proposed, via, e.g., Riemannian optimization [28], convex relaxation [21], and mixed-integer programming [14]. While globally optimal, these methods all come at a much higher computational cost than vanilla ICP. This was, to some degree, addressed by the Fast Global Registration (FGR) algorithm [49], which leverages a local refinement strategy to speed up computation. While effective, FGR still suffers from the presence of noise and outliers in the point sets, particularly because, as vanilla ICP, it simply relies on 3D point-to-point distance to establish correspondences. In principle, this can be addressed by designing point descriptors that can be more robustly matched. Over the years, several works have tackled this task, in both a non learning-based [15, 31, 30] and learning-based [48, 16] fashion. Nowadays, however, these approaches are outperformed by end-to-end learning frameworks, which directly take the point sets as input.

**End-to-end learning with point sets.** A key requirement to enable end-to-end learning-based registration was the design of deep networks acting on unstructured sets. Deep sets [47] and PointNet [25] constitute the pioneering works in this direction. They use shared multilayer perceptrons to extract high-dimensional features from the input point coordinates, and exploit a symmetric function to aggregate these features. This idea was then extended in PointNet++ [26] via a modified sampling strategy to robustify the network to point clouds of varying density, in DGCNN [40] by building a graph over the point cloud, in PointCNN [18] by learning a transformation of the data so as to be able to process it with standard convolutional layers, and in PCNN [2] via an additional extension operator before applying the convolutions. While the above-mentioned works focused on other tasks than us, such as point cloud classification or segmentation, end-to-end

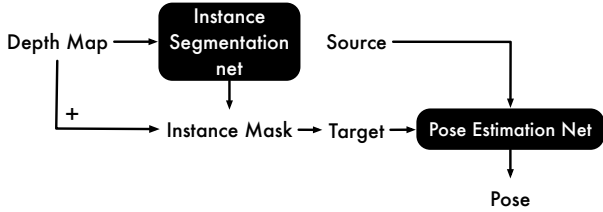


Figure 2: Illustration of our framework.

learning for registration has recently attracted a growing attention. In particular, PointNetLK [1] combines the PointNet backbone with the traditional, iterative Lucas-Kanade (LK) algorithm [20] so as to form an end-to-end registration network; DCP [38] exploits DGCNN backbones followed by Transformers [35] to establish 3D-3D correspondences, which are then passed through an SVD layer to obtain the final rigid transformation. While effective, PointNetLK and DCP cannot tackle the partial-to-partial registration scenario. That is, they assume that both point sets are fully observed, during both training and test time. This was addressed by PRNet [39] via a deep network designed to extract keypoints from each input set and match these keypoints. This network is then applied in an iterative manner, so as to increasingly refine the resulting transformation. Similarly, RPM-Net [45] builds on DCP, replacing its softmax layer with an optimal transport one so as to handle outliers, and as PRNet, relies on an iterative strategy to refine the computed transformation. In any event, the methods discussed above were designed to handle point-clouds in full 3D, and were thus not demonstrated for registration from 2.5D measurements. By contrast, DGR [7], which uses a deep network to reject the outliers from an input set of correspondences, was shown to be applicable to depth data. Nevertheless, this was achieved in the context of registering two partial views of a scene, whereas we focus on estimating the 6D pose of an object captured in a scene.

To the best of our knowledge, only few methods have been proposed to address this challenging scenario. In particular, [36] relies on generating pose hypotheses via feature matching, followed by a RANSAC-inspired method to choose the candidate pose with the largest number of support matches. Similarly, TEASER [42] and its improved version TEASER++ [43] take putative correspondences obtained via feature matching as input and remove the outlier ones by an adaptive voting scheme. By relying on hand-crafted features designed for 3D point-clouds, these methods do not explicitly address the case of 2.5D measurements. This is what we address in this work, and, motivated by the great progress of deep networks to address the classical 3D registration scenario, introduce the first deep learning framework capable of estimating the 6D pose of a 3D object observed with a 2.5D sensor in a scene.

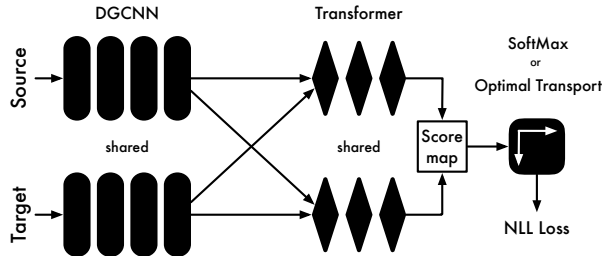


Figure 3: Architecture of the pose estimation network.

### 3. Methodology

Let us now introduce our approach to estimating the 6D pose of an object, represented with a reference point cloud in full 3D, from 2.5D observations of this object in a scene. To address this challenging scenario, we develop the deep learning framework depicted by Fig. 2. It relies on two main modules, an instance segmentation network and a pose estimation network, which we discuss in detail below.

#### 3.1. Instance Segmentation

To tackle the realistic scenario where the object is immersed in a scene, we first process the input depth map with an instance segmentation module. Specifically, we build on the YOLACT [5] framework that has proven highly effective for image-based instance segmentation. To exploit this framework in our scenario, we replicate the depth map  $I_{depth}$  three times, so as to obtain 3 channels, as an RGB image, which allows us to benefit from the pre-training of the model on an image dataset. Furthermore, instead of predicting multiple object categories, we train our model to discriminate between object and background, which we found to be better suited to handle depth that does not carry appearance information. Note that we nonetheless train our model using multiple object categories. Finally, after non-maximum suppression, we only keep the bounding box with the highest score, which we observed to work well in practice, as will be shown by our experiments, and as evidenced qualitatively in Fig. 4. Ultimately, our instance segmentation module produces a mask image, expressed as

$$I_{mask} = \phi_{seg}(I_{depth}). \quad (1)$$

We then use  $I_{mask}$  to isolate the target point cloud, which we input to the pose estimation network described below.

#### 3.2. Pose Estimation

Let us now turn to the task of estimating the 6D pose of the object of interest. To this end, let  $\mathcal{X} \in \mathbb{R}^{M \times 3}$  and  $\mathcal{Y} \in \mathbb{R}^{N \times 3}$  be two sets of 3D points sampled from the same object surface. We typically refer to  $\mathcal{X}$  as the source point set and to  $\mathcal{Y}$  as the target point set. We obtain the source point set  $\mathcal{X}$  by uniform sampling from the mesh model, and

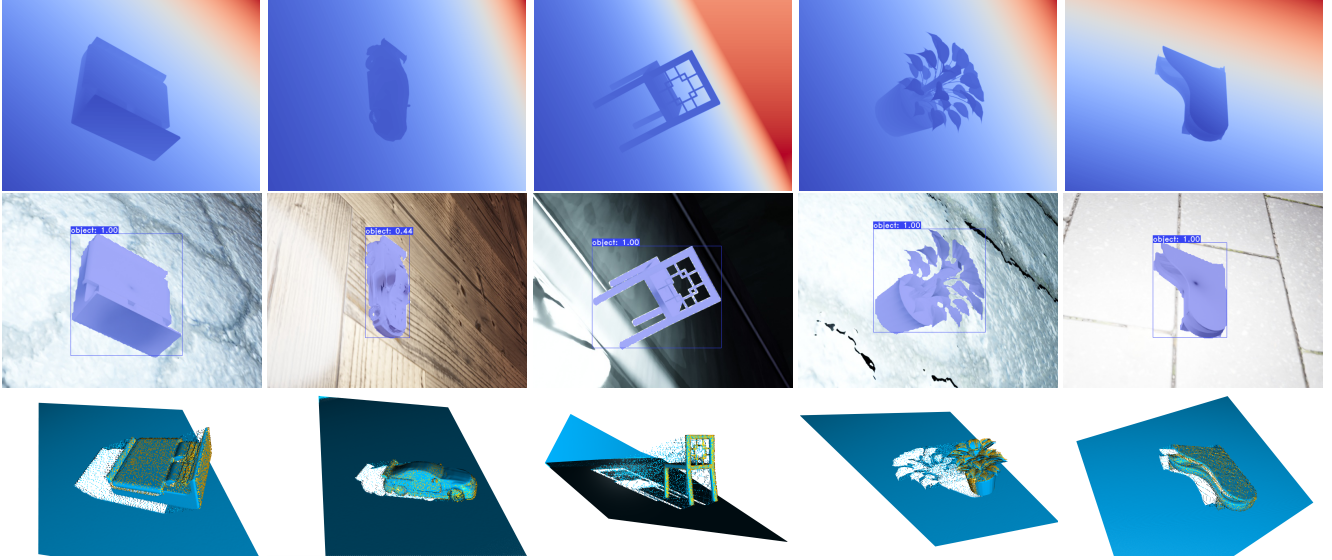


Figure 4: Qualitative results. (Top) Test depth map used as input to our instance segmentation module. (Middle) Resulting predicted instance mask. (Bottom) Final pose estimation result (Ours-OT).

target one  $\mathcal{Y}$  from  $I_{depth}$  and  $I_{mask}$ , assuming known camera intrinsic parameters. Registration then aims to find a rigid transformation  $\mathcal{T}$  that aligns  $\mathcal{X}$  to  $\mathcal{Y}$ . In this work, we focus on the case where the object is self-occluded. To be specific, we assume that each point in  $\mathcal{Y}$  has a corresponding point in  $\mathcal{X}$ , but not the opposite.

We build our pose estimation module on DCP [38], extending it to handle the partial correspondence scenario. As illustrated in Fig. 3, we rely on the DCP-v2 design, which consists of a DGCNN [40] followed by a Transformer [35]. Specifically, the DGCNN takes a point set as input, constructs a k-NN graph from it, and then extracts point-wise features via standard convolutions on this graph, encoding diverse levels of context by max-pooling the local features and concatenating the resulting representations to the point-wise ones. Let  $\theta^x$ , resp.  $\theta^y$ , be the final feature matrix, i.e., one  $P$ -dimensional feature vector per 3D point, for  $\mathcal{X}$ , resp.  $\mathcal{Y}$ . The transformer then learns a function  $\phi : \mathbb{R}^{M \times P} \times \mathbb{R}^{N \times P} \rightarrow \mathbb{R}^{M \times P}$ , that combines the information of the two point sets. Ultimately, this produces descriptor matrices  $\mathbf{f}^x$ , resp.  $\mathbf{f}^y$ , for  $\mathcal{X}$ , resp.  $\mathcal{Y}$ , written as

$$\mathbf{f}^x = \theta^x + \phi(\theta^x, \theta^y), \quad \mathbf{f}^y = \theta^y + \phi(\theta^y, \theta^x). \quad (2)$$

Given these matrices, we then form a score map  $\mathcal{S} \in \mathbb{R}^{M \times N}$  by computing the similarity between each source-target pair of descriptors. That is, we compute the  $(i, j)$ -th element of  $\mathcal{S}$  as

$$\mathcal{S}_{i,j} = \langle \mathbf{f}_i^x, \mathbf{f}_j^y \rangle, \quad \forall (i, j) \in [1, M] \times [1, N], \quad (3)$$

where  $\langle \cdot, \cdot \rangle$  is the inner product, and  $\mathbf{f}_i^x, \mathbf{f}_j^y \in \mathbb{R}^P$ .

In DCP [38], this score map is passed through a row-wise softmax so as to obtain correspondences. These cor-

respondences are then processed within the network via an SVD layer to solve the Procrustes problem, and the resulting rigid transformation is compared to the ground-truth one with a mean squared error (MSE) loss. Here, when  $I_{mask}$  can be assumed to be clean, we keep the softmax because each point in  $\mathcal{Y}$  should be visible in  $\mathcal{X}$ . However, we remove the SVD layer, which, if not carefully designed, can make the training process unstable [9, 10, 37, 45]. Instead, we impose direct supervision on the output of the softmax. To this end, let  $\mathcal{M} \in \{0, 1\}^{M \times N}$  be the matrix of ground-truth correspondences, with a 1 indicating a correspondence between a pair of points. Such correspondences can be estimated using the ground-truth transformation matrix, as discussed in more detail in Section 4.1. We then express our loss function as the negative log-likelihood

$$\mathcal{L}(\mathcal{P}, \mathcal{M}) = \frac{-\sum_{i=1}^M \sum_{j=1}^N (\log \mathcal{P}_{i,j}) \mathcal{M}_{i,j}}{\sum_{i=1}^M \sum_{j=1}^N \mathcal{M}_{i,j}}, \quad (4)$$

where  $\mathcal{P}$  is the output of the softmax, and where the denominator normalizes the loss value so that different training samples containing different number of correspondences have the same influence in the overall empirical risk.

**Dealing with noisy target points.** Although the softmax works well when the points in  $\mathcal{Y}$  all have a corresponding point in  $\mathcal{X}$ , in practice,  $\mathcal{Y}$  may include noise, due, for example, to an imperfect  $I_{mask}$  prediction. To address this, we replace the softmax with an optimal transport layer [45, 32] including an outlier bin to handle the noise.

Specifically, we extend the score matrix  $\mathcal{S}$  by one row

---

**Algorithm 1:** Log-domain Sinkhorn’s algorithm.

---

**Input** :  $\bar{\mathcal{S}}, \mathbf{a} = [\mathbb{1}_M^\top, N]^\top, \mathbf{b} = [\mathbb{1}_N^\top, M]^\top,$   
 $\mathbf{f}_0 = \mathbb{0}_{M+1}, \mathbf{g}_0 = \mathbb{0}_{N+1},$   
 $\lambda$  and  $k$  (number of iterations)  
**Output:** Assignment matrix  $\bar{\mathcal{P}}$   
**Init** :  $\bar{\mathcal{S}} = -\bar{\mathcal{S}}/\lambda$   
**while**  $l \leq k$  **do**  
     $\mathbf{f}^{(l+1)} = \lambda \log(\mathbf{a}) - \text{logsumexp}(\bar{\mathcal{S}} + \mathbb{1}_{N+1} \mathbf{g}^{(l)\top})$   
     $\mathbf{g}^{(l+1)} =$   
     $\lambda \log(\mathbf{b}) - \text{logsumexp}(\bar{\mathcal{S}} + \mathbf{f}^{(l+1)} \mathbb{1}_{M+1}^\top)$   
**end**  
 $\bar{\mathcal{P}}_{i,j} = \exp(\bar{\mathcal{S}}_{i,j} + \mathbf{f}_i + \mathbf{g}_j); \triangleright$  transfer back  
to the original domain.

---

and one column to form an augmented score matrix  $\bar{\mathcal{S}}$ . The values at the newly-created positions in  $\bar{\mathcal{S}}$  are set to

$$\bar{\mathcal{S}}_{i,N+1} = \bar{\mathcal{S}}_{M+1,j} = \bar{\mathcal{S}}_{M+1,N+1} = \alpha, \quad (5)$$

$\forall i \in [1, M], \forall j \in [1, N]$ , where  $\alpha \in \mathbb{R}$  is a fixed parameter, which set to be 0.01 in practice. The values at the other indices directly come from  $\mathcal{S}$ . Given the augmented score map  $\bar{\mathcal{S}}$ , we aim to find a partial assignment  $\bar{\mathcal{P}} \in \mathbb{R}^{(M+1) \times (N+1)}$ , defining correspondences between the two point sets, extended with the outlier bins. Let  $\mathbf{U}(\mathbf{a}, \mathbf{b})$  be the set of probability matrices defined as

$$\left\{ \bar{\mathcal{P}} \in \mathbb{R}_+^{(M+1) \times (N+1)} : \bar{\mathcal{P}} \mathbb{1}_{M+1} = \mathbf{a} \text{ and } \bar{\mathcal{P}}^\top \mathbb{1}_{N+1} = \mathbf{b} \right\}, \quad (6)$$

where  $\mathbf{a} = [\mathbb{1}_M^\top, N]^\top$ , and  $\mathbf{b} = [\mathbb{1}_N^\top, M]^\top$ , with  $\mathbb{1}_M = [1, 1, \dots, 1]^\top \in \mathbb{R}^M$ . Then, from the optimal transport theory [23, 8], an assignment probability matrix  $\bar{\mathcal{P}}$  can be obtained by solving

$$\min_{\bar{\mathcal{P}} \in \mathbf{U}(\mathbf{a}, \mathbf{b})} \langle \bar{\mathcal{S}}, \bar{\mathcal{P}} \rangle - \lambda E(\bar{\mathcal{P}}), \quad (7)$$

where  $\langle \cdot, \cdot \rangle$  is the Frobenius dot product and  $E(\cdot)$  is an entropy regularization term defined as  $E(\bar{\mathcal{P}}) = -\sum_{i,j} \bar{\mathcal{P}}_{i,j} (\log(\bar{\mathcal{P}}_{i,j}) - 1)$ . In practice, this optimization

problem can be solved by using the log-domain Sinkhorn algorithm, which we summarized in Algorithm 1, where the matrix operator  $\text{logsumexp}(\mathcal{A}) = \log(\exp(\mathcal{A}_{1,1}) + \dots + \exp(\mathcal{A}_{i,j}) + \dots + \exp(\mathcal{A}_{M,N}))$ . Since all operations performed by this algorithm are differentiable, the training errors can be backpropagated to the rest of the network. We then still use the negative log-likelihood of Eq. 4 as loss function, but replacing  $\mathcal{M}$  with  $\bar{\mathcal{M}}$ , which contains an extra row and column acting as outlier bins.

### 3.3. Training via On-the-fly Rendering

To train our network, we follow a two-stage procedure, starting with the instance segmentation module and following with the pose estimation one. Unfortunately, there exist

virtually no real dataset providing high-quality depth data for 6D object pose estimation in context. For instance, the datasets in the BOP challenge [13] mostly provide relatively low-quality depth maps, with very sparse depth measurements for the object. Such low-quality depth observations, however, are not representative of the resolutions that modern sensors can now achieve [19]. To better reflect the progress of these sensors, in this work, we rely on BlenderProc [11] to generate high-quality synthetic data, as will be discussed in more detail in Section 4.2. However, even such synthetic data remains imperfect at the object boundaries, mixing the object depth with the background one, as shown in Fig. 7. Such outliers at the boundaries affect the training process, and we therefore use BlenderProc to train our instance segmentation module but not our pose estimation one. Instead, and to simultaneously benefit from having access to virtually infinite amounts of training data, we follow an on-the-fly rendering strategy. Specifically, we use Pytorch3D [27] to generate scenes that contain individual objects without background, thus fulfilling the pose estimation network’s assumption and precluding the presence of outliers at the object boundaries. The use of Pytorch3D allows us to interface the rendering process with the network training, thus preventing the need to generate and store a fixed set of training samples in a pre-processing stage.

## 4. Experiment

We first compare our approach to the state-of-the-art methods on the task of estimating the pose of a self-occluded object without a scene background, and then turn to the more challenging scenario where the object is immersed in context. Finally we analyze the influence of the different components of our approach.

### 4.1. Self-Occluded Object Registration without Background

**Dataset.** For this experiment, we use the auto-aligned ModelNet40 dataset [41, 33]. This dataset contains mesh models for 40 object categories. The point clouds are normalized in the range  $[-1, 1]$  on each axis. As in [39], we split the data into 9,843 training and 2,468 testing mesh models. We use the mesh models to render depth maps given camera viewpoints and intrinsic parameters. Specifically, we treat the full point clouds corresponding to the meshes as source sets  $\mathcal{X}$  and the resulting depth maps as target sets  $\mathcal{Y}$ . We use the look-at method<sup>1</sup> to place the camera, and set the distance between the camera and the center of the object to be 0.65. We then randomly sample the elevation in  $[15^\circ, 75^\circ]$  and azimuth in  $[0^\circ, 89^\circ]$ . To deal with the large number of points, following [7, 43], we first voxelize the point clouds with a voxel size of  $0.05 \times (\frac{\sqrt{2}}{2})$ , and

<sup>1</sup><https://www.scratchapixel.com/lessons/mathematics-physics-for-computer-graphics/lookat-function>

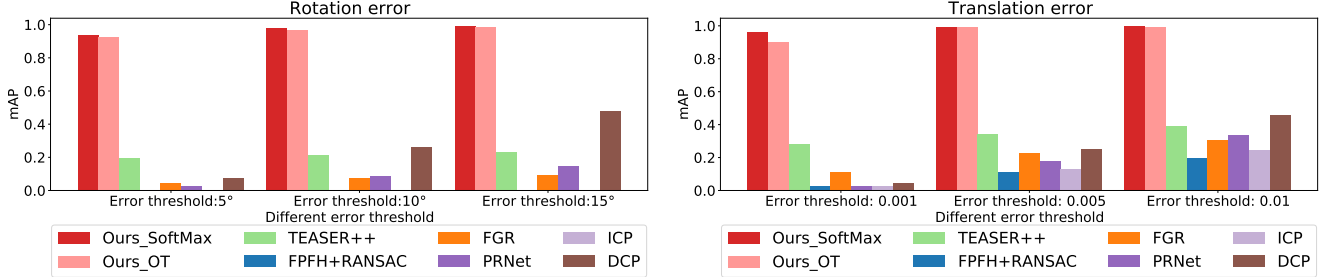


Figure 5: Rotation and translation mAP for different thresholds on the ModelNet40 dataset without background.

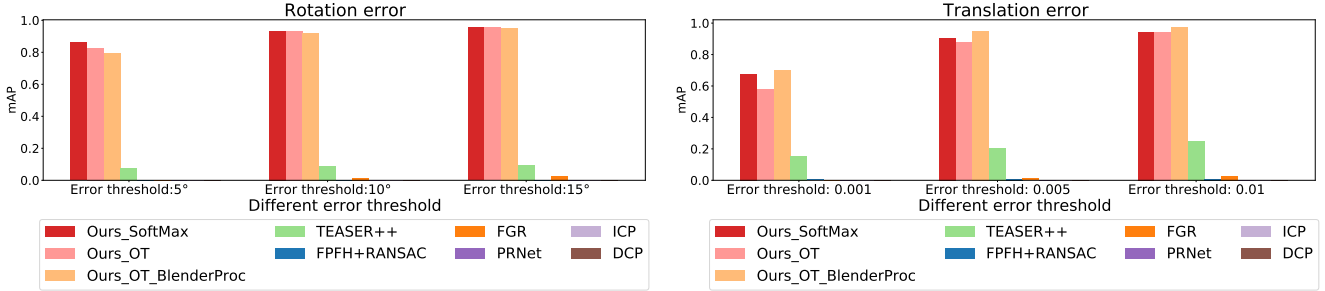


Figure 6: Rotation and translation mAP for different thresholds on the ModelNet40 dataset with background.

then randomly sample the desired number of points from the voxelized point clouds.

**Evaluation metrics.** We report the rotation error and translation error between the predictions  $\hat{R}, \hat{\mathbf{t}}$  and the ground truth  $R_{gt}, \mathbf{t}_{gt}$ . These errors are computed as

$$E_{rot}(\hat{R}, R_{gt}) = \arccos \frac{\text{trace}(\hat{R}^\top R_{gt}) - 1}{2}, \quad (8)$$

$$E_{trans}(\hat{\mathbf{t}}, \mathbf{t}_{gt}) = \|\hat{\mathbf{t}} - \mathbf{t}_{gt}\|_2^2.$$

We summarize the results in terms of mean average precision (mAP) of the estimated relative pose under varying accuracy thresholds, as in [46]. For the rotation, we use the three thresholds  $[5^\circ, 10^\circ, 15^\circ]$ , and for the translation, we set the thresholds to be  $[1 \times 10^{-3}, 5 \times 10^{-3}, 1 \times 10^{-2}]$ .

**Implementation details.** We implement our pose estimation network in Pytorch [22] and train it from scratch. We use the Adam optimizer [17] with a learning rate of  $10^{-3}$  and mini-batches of size 20, and train the network for 40,000 iterations. We set the number of points for  $\mathcal{X}$  and  $\mathcal{Y}$  to be 1024 and 768, respectively, encoding the fact that  $\mathcal{Y}$  only contains a visible portion of  $\mathcal{X}$ . We use the same parameters for both Ours\_SoftMax and Ours\_OT. For the OT layer, we use  $k = 50$  iterations and set  $\lambda = 0.5$ . Training was performed on one NVIDIA RTX8000 GPU.

To build the ground-truth assignment matrix  $\mathcal{M}$  for Ours\_SoftMax and Ours\_OT, we transform  $\mathcal{X}$  using the ground-truth transformation  $\mathcal{T}$ , giving us  $\tilde{\mathcal{X}}$ . We then compute the pairwise Euclidean distance matrix between  $\tilde{\mathcal{X}}$  and  $\mathcal{Y}$ , which we threshold to 0.05 to obtain a correspondence matrix  $\mathcal{M} \in \{0, 1\}$ . For Ours\_OT, we augment  $\mathcal{M}$  with an extra row and column acting as outlier bins to obtain  $\tilde{\mathcal{M}}$ .

The points without any correspondence are treated as outliers, and the corresponding positions in  $\tilde{\mathcal{M}}$  are set to one. This strategy does not guarantee a bipartite matching, which we address using a forward-backward check.

**Registration results.** We compare our approach to PRNet [39], DCP [38], ICP [3], PPFH-RANSAC [30], FGR [49] and TEASER++ [42, 43]. Note that, despite our best effort, we were unable to successfully train DGR [7] on our dataset. We believe this to be due to the different nature of the task addressed by DGR, i.e., scene to scene registration. This is further evidenced by the fact that, in [7], the DGR authors mentioned that they were unable to train DCP on the 3DMatch dataset [48], whereas we underwent not problems with DCP in our scenario. Similarly, we were unable to train RPMNet [45] on our data, encountering the instabilities reported by the RPMNet authors, with training crashing after 10 epochs because of an error during SVD.

For the PRNet, we use the pretrained partial-to-partial model provided by the authors, which we fine-tune on our dataset with a learning rate of 0.0001 for 10 epochs, where we observed convergence. For DCP, we use the pretrained DCP-v2 model (clean version), and similarly fine-tune it on our dataset with a learning rate of 0.001 for 30 epochs corresponding to convergence. For ICP, PPFH-RANSAC and FGR, we use the Open3D [50] implementations. For TEASER++ we use the official implementation.

The results are summarized in Fig. 5. Our methods outperforms all the baselines in all settings, with our two variants yielding similar results. TEASER++ achieves the best result among the baselines for a threshold of  $5^\circ$ , but is outperformed by DCP for  $10^\circ$  and  $15^\circ$ , which justifies our choice of DCP as our base network. We believe this to illus-

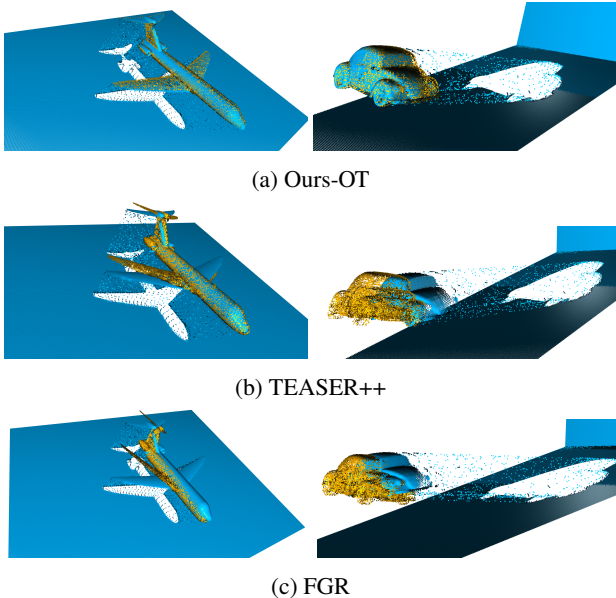


Figure 7: Qualitative results on the BlenderProc dataset. Note that our approach (Ours-OT) yields much more precise registrations than the two top-performing baselines.

trate a downside of exploiting handcrafted features, such as FPFH, as TEASER++ does; while such features are reliable for some objects, they do not generalize well to all of them. By contrast, deep networks can learn to leverage different sources of information for different objects. We attribute the relatively poor performance of PRNet to the fact that it was designed specifically for object-to-object registration.

## 4.2. Self-Occluded Object Pose Estimation with Background

Let us now turn to the more challenging scenario where the object is immersed in a scene.

**Dataset.** To this end, we generate a dataset using the BlenderProc [11] photo-realistic renderer discussed in Section 3.3. Specifically, we create cubic scenes of length 4 with random texture images from the CC0textures dataset<sup>2</sup>. In each scene, we place an object from the ModelNet40 dataset [41] with a randomly sampled elevation and azimuth. We then render depth maps from given cameras, together with a mask of the object’s visible portion, and the object pose and bounding box. We follow the same procedure to generate the training and test data, using the same object splits and the same sampling range for the look-at camera model as in Section 4.1.

The main difference between this experiment and the previous one is that the algorithms must identify the object in the scene. The whole scene contains  $640 \times 480$  points, which after voxelization still leaves between 15,000 and 300,000 points. Among these, the object itself covers

<sup>2</sup><https://cc0textures.com>

only 1,000 to 9,000 points, depending on the structure of the mesh model. This corresponds to an inlier rate ranging from 0.5% to 23.5%, with 79.41% of the samples having an inlier rate less than 5%.

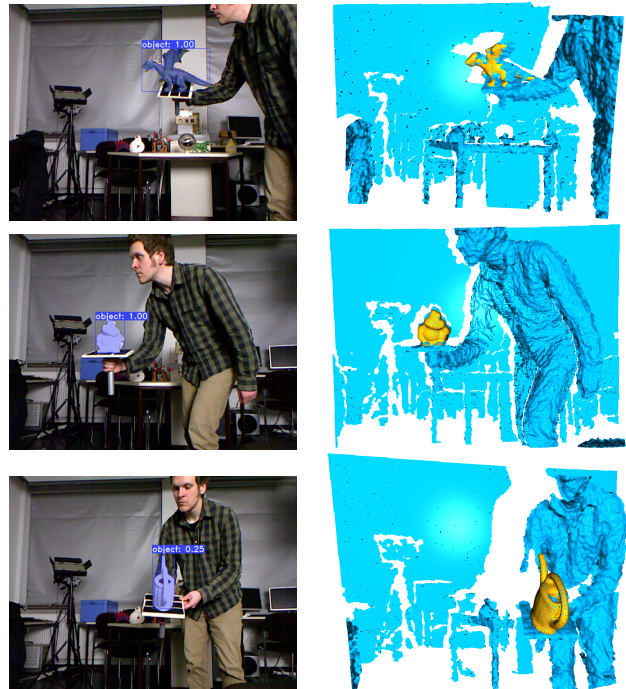


Figure 8: Qualitative results on the TUD-L dataset. (Left) Mask produced by our instance segmentation module. (Right) Object model registered to the input depth map using the pose predicted by Ours-OT.

**Implementation details.** For our instance segmentation network, we use a pre-trained Resnet101 backbone [12]. Since the input to our model is not an image, we replicate the depth map three times to match the number of input channels. As output, we keep only one category, which is used to classify each pixel as belonging to the object or not. We train the resulting network for 100,000 iterations with mini-batches of size 16, and using SGD with a learning rate of  $10^{-3}$ . We then train our pose estimation module in the same manner as in Section 4.1, but discarding the points that do not belong to the object using the ground-truth mask. This, of course, can only be achieved during training, and leads to a mismatch between training and testing time, since, at testing time, we cannot expect our instance segmentation module to always give perfect results. To handle this, at test time, we erode the boundary of the predicted masks with a  $3 \times 3$  kernel. Furthermore, we remove all the points that lie outside a sphere centered on the object and of radius 1.2, accounting for the fact that the object coordinates were normalized in the range  $[-1, 1]$ .

**Registration results.** We compare our approach to the same baselines as in Section 4.1, using the same hyper-

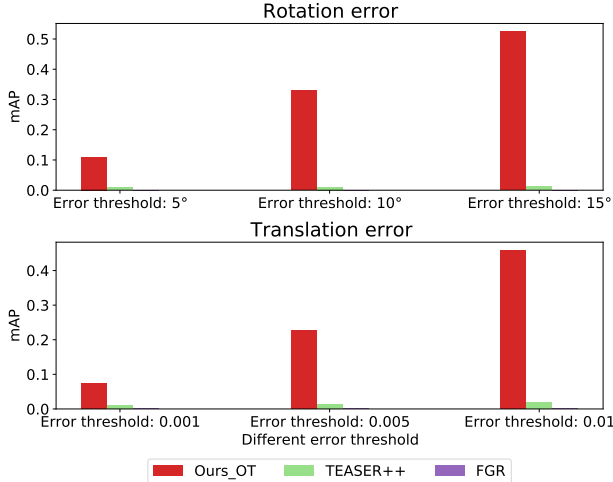


Figure 9: Rotation and translation mAP for different thresholds on the TUD-L dataset.

parameter values to train them. The only exception to this is for TEASER++, for which we limit the number of points in the target point set to a maximum of 50,000 because we observed too large target point sets to produce a segmentation fault in the code. Note that, prior to our work, no method was designed to explicitly estimate the 6D pose of a self-occluded object observed in a scene. Therefore, the baselines directly tackle the 3D registration task from the raw depth maps. By contrast, our segmentation module outputs a mask that facilitates the task of the registration one.

The results are summarized in Fig. 6, with a few examples in Fig. 7. Note that our methods outperform the baselines by a large margin. Since the DCP and PRNet directly act on the raw depth maps, the point-cloud downsampling process, required to make inference tractable, leaves only very few points belonging to the object, thus leading to the failure of these methods. By contrast, TEASER++, which was designed to handle such large amounts of outliers, yields reasonable results, nevertheless clearly outperformed by our learning-based strategy.

### 4.3. Dealing with Real Data

To evidence that our approach generalizes to real depth maps, we use the TUD-L dataset [13], which contains training and testing image sequences that show three moving objects under eight lighting conditions. We retrain our complete model with OT layer from scratch on this dataset, keeping the same hyper-parameter values as for the previous experiments. To compare our method to the baselines, we select 2000 images from each testing sequence. We restrict our baseline evaluation to the methods that gave reasonable results in the experiment of Section 4.1, i.e., TEASER++ and FGR. As can be shown in Fig. 9, our method also outperforms the baselines by a large margin in this scenario. In

Methods	512	1024	2048
ICP	0.018	0.028	0.054
FGR	0.032	0.059	0.132
TEASER++	0.025	0.085	0.249
DCP	0.013	0.018	0.053
PRNet	0.051	0.075	0.141
Ours-OT	0.033	0.052	0.112

Table 1: Inference time (in seconds).

Fig. 8, we show a few qualitative results obtained with our framework, evidencing the accuracy of our predictions.

### 4.4. Method Analysis

**Inference Time.** In Table 1, we compare the inference time of our registration method to that of the baselines for different point set sizes. For this comparison to be fair, we ran all methods on a desktop computer with an Intel(R) Core(TM) i7-7700K CPU @ 4.20GHz, an Nvidia GTX 2080 Ti GPU, and 32GB memory. Theoretically, the inference time for Ours\_SoftMax is the same as DCP, thus we omit it. Ours\_OT yields run-times comparable to FGR, while being slightly faster than PRNet. Note that the run-times reported in Table 1 for our approach do not include the instance segmentation module, which takes 0.0285s to process an image of size  $480 \times 640$ .

**Effectiveness of the Optimal Transport Layer.** Note that the best results with our approach were obtained without the optimal transport layer. Here, we illustrate that this layer is nonetheless important in scenarios where the training data is noisy. To this end, we replace our rendering on-the-fly procedure with BlenderProc during training so as to generate noisy training observations. To be specific, we use the ground-truth mask to obtain the depth of the object and transform it to the target point cloud, and then jitter the rotation in the range  $[0, 45^\circ]$  and the translation in the range  $[-1, 1]$  on each axis. Only Ours\_OT could be trained on the resulting dataset, thanks to its outlier bins. We provide the corresponding results as Ours\_OT\_BlenderProc in Fig. 6.

## 5. Conclusion

We have introduced the first learning-based approach to estimating the 6D pose of a self-occluded object immersed in a scene. Our method is intuitive, relying on an instance segmentation module followed by a pose estimation one. As evidenced by our empirical results, this strategy is effective, outperforming the state-of-the-art traditional and learning-based methods, which so far have mostly focused on registering partial views of the same object or scene. We believe that the problem we have tackled here is central in many practical applications. In particular, in the future, we will aim to deploy our approach for LiDAR-based registration in the context of non-cooperative rendezvous in space.

## References

- [1] Yasuhiro Aoki, Hunter Goforth, Rangaprasad Arun Srivatsan, and Simon Lucey. Pointnetlk: Robust & efficient point cloud registration using pointnet. In *Conference on Computer Vision and Pattern Recognition*, pages 7163–7172, 2019. 1, 3
- [2] Matan Atzmon, Haggai Maron, and Yaron Lipman. Point convolutional neural networks by extension operators. In *ACM Transactions on Graphics (TOG)*, 2018. 2
- [3] P. Besl and N. McKay. A method for registration of 3d shapes. *IEEE Transactions on Pattern Analysis and Machine Intelligence*, 14(2):239–256, February 1992. 6
- [4] Paul J Besl and Neil D McKay. Method for registration of 3-d shapes. In *Sensor fusion IV: control paradigms and data structures*, volume 1611, pages 586–606. International Society for Optics and Photonics, 1992. 1
- [5] Daniel Bolya, Chong Zhou, Fanyi Xiao, and Yong Jae Lee. Yolact: Real-time instance segmentation. In *Conference on Computer Vision and Pattern Recognition*, pages 9157–9166, 2019. 3
- [6] Sofien Bouaziz, Andrea Tagliasacchi, and Mark Pauly. Sparse iterative closest point. In *Computer graphics forum*, volume 32, pages 113–123. Wiley Online Library, 2013. 2
- [7] Christopher Choy, Wei Dong, and Vladlen Koltun. Deep global registration. In *Proceedings of the IEEE Conference on Computer Vision and Pattern Recognition*, 2020. 1, 3, 5, 6
- [8] Marco Cuturi. Sinkhorn distances: Lightspeed computation of optimal transport. In *NIPS*, pages 2292–2300, 2013. 5
- [9] Zheng Dang, Kwang Moo Yi, Yinlin Hu, Fei Wang, Pascal Fua, and Mathieu Salzmann. Eigendecomposition-free training of deep networks with zero eigenvalue-based losses. In *European Conference on Computer Vision*, pages 768–783, 2018. 4
- [10] Z. Dang, K. M. Yi, Y. Hu, F. Wang, P. Fua, and M. Salzmann. Eigendecomposition-free training of deep networks for linear least-square problems. *IEEE Transactions on Pattern Analysis and Machine Intelligence*, 16, 2020. 4
- [11] Maximilian Denninger, Martin Sundermeyer, Dominik Winkelbauer, Youssef Zidan, Dmitry Olefir, Mohamad Elbadrawy, Ahsan Lodhi, and Harinandan Katam. Blenderproc. In *arXiv Preprint*, 2019. 2, 5, 7
- [12] Kaiming He, Xiangyu Zhang, Shaoqing Ren, and Jian Sun. Deep residual learning for image recognition. In *Proceedings of the IEEE conference on computer vision and pattern recognition*, pages 770–778, 2016. 7
- [13] Tomas Hodan, Frank Michel, Eric Brachmann, Wadim Kehl, Anders GlentBuch, Dirk Kraft, Bertram Drost, Joel Vidal, Stephan Ihrke, Xenophon Zabulis, et al. Bop: Benchmark for 6d object pose estimation. In *European Conference on Computer Vision*, pages 19–34, 2018. 5, 8
- [14] Gregory Izatt, Hongkai Dai, and Russ Tedrake. Globally optimal object pose estimation in point clouds with mixed-integer programming. In *Robotics Research*, pages 695–710. Springer, 2020. 2
- [15] Andrew E. Johnson and Martial Hebert. Using spin images for efficient object recognition in cluttered 3d scenes. *TPAMI*, 21(5):433–449, 1999. 2
- [16] Marc Khoury, Qian-Yi Zhou, and Vladlen Koltun. Learning compact geometric features. In *International Conference on Computer Vision*, pages 153–161, 2017. 2
- [17] Diederik P Kingma and Jimmy Ba. Adam: A method for stochastic optimization. In *International Conference on Learning Representations*, 2015. 6
- [18] Yangyan Li, Rui Bu, Mingchao Sun, Wei Wu, Xinhan Di, and Baoquan Chen. Pointcnn: Convolution on x-transformed points. In *Advances in Neural Information Processing Systems*, pages 820–830, 2018. 2
- [19] MingLei Lu, Yu Guo, Fei Wang, and Zheng Dang. A method to generate high precision mesh model and rgb-d dataset for 6d pose estimation task. *arXiv preprint*, 2020. 5
- [20] Bruce D Lucas, Takeo Kanade, et al. An iterative image registration technique with an application to stereo vision. In *International Joint Conference on Artificial Intelligence*. Vancouver, British Columbia, 1981. 3
- [21] Haggai Maron, Nadav Dym, Itay Kezurer, Shahar Kovalsky, and Yaron Lipman. Point registration via efficient convex relaxation. *ACM Transactions on Graphics (TOG)*, 35(4):1–12, 2016. 2
- [22] Adam Paszke, Sam Gross, Soumith Chintala, Gregory Chanan, Edward Yang, Zachary DeVito, Zeming Lin, Alban Desmaison, Luca Antiga, and Adam Lerer. Automatic differentiation in pytorch. In *International Conference on Learning Representations*, 2017. 6
- [23] Gabriel Peyré, Marco Cuturi, et al. Computational optimal transport. *Foundations and Trends® in Machine Learning*, 11(5-6):355–607, 2019. 5
- [24] François Pomerleau, Francis Colas, Roland Siegwart, et al. A review of point cloud registration algorithms for mobile robotics. *Foundations and Trends® in Robotics*, 4(1):1–104, 2015. 2
- [25] C.R. Qi, H. Su, K. Mo, and L.J. Guibas. Pointnet: Deep learning on point sets for 3d classification and segmentation. In *Conference on Computer Vision and Pattern Recognition*, 2017. 2
- [26] C.R. Qi, L. Yi, H. Su, and L.J. Guibas. Pointnet++: Deep hierarchical feature learning on point sets in a metric space. In *Advances in Neural Information Processing Systems*, 2017. 2
- [27] Nikhila Ravi, Jeremy Reizenstein, David Novotny, Taylor Gordon, Wan-Yen Lo, Justin Johnson, and Georgia Gkioxari. Accelerating 3d deep learning with pytorch3d. *arXiv preprint arXiv:2007.08501*, 2020. 5
- [28] David M Rosen, Luca Carlone, Afonso S Bandeira, and John J Leonard. Se-sync: A certifiably correct algorithm for synchronization over the special euclidean group. *The International Journal of Robotics Research*, 38(2-3):95–125, 2019. 2
- [29] Szymon Rusinkiewicz and Marc Levoy. Efficient variants of the icp algorithm. In *Proceedings Third International Conference on 3-D Digital Imaging and Modeling*, pages 145–152. IEEE, 2001. 2

- [30] Radu Bogdan Rusu, Nico Blodow, and Michael Beetz. Fast point feature histograms (fpfh) for 3d registration. In *International Conference on Robotics and Automation*, pages 3212–3217. IEEE, 2009. 2, 6
- [31] Radu Bogdan Rusu, Nico Blodow, Zoltan Csaba Marton, and Michael Beetz. Aligning point cloud views using persistent feature histograms. In *International Conference on Intelligent Robots and Systems*, pages 3384–3391. IEEE, 2008. 2
- [32] Paul-Edouard Sarlin, Daniel DeTone, Tomasz Malisiewicz, and Andrew Rabinovich. Superglue: Learning feature matching with graph neural networks. In *Conference on Computer Vision and Pattern Recognition*, 2019. 4
- [33] Nima Sedaghat, Mohammadreza Zolfaghari, Ehsan Amiri, and Thomas Brox. Orientation-boosted voxel nets for 3d object recognition. In *British Machine Vision Conference*, 2016. 5
- [34] Aleksandr Segal, Dirk Haehnel, and Sebastian Thrun. Generalized-icp. In *In Robotics: Science and Systems*, 2009. 2
- [35] Ashish Vaswani, Noam Shazeer, Niki Parmar, Jakob Uszkoreit, Llion Jones, Aidan N Gomez, Łukasz Kaiser, and Illia Polosukhin. Attention is all you need. In *Advances in Neural Information Processing Systems*, pages 5998–6008, 2017. 3, 4
- [36] Joel Vidal, Chyi-Yeu Lin, Xavier Lladó, and Robert Martí. A method for 6d pose estimation of free-form rigid objects using point pair features on range data. *Sensors*, 18(8):2678, 2018. 2, 3
- [37] Wei Wang, Zheng Dang, Yinlin Hu, Pascal Fua, and Mathieu Salzmann. Backpropagation-friendly eigendecomposition. In *Advances in Neural Information Processing Systems*, pages 3156–3164, 2019. 4
- [38] Yue Wang and Justin M Solomon. Deep closest point: Learning representations for point cloud registration. In *International Conference on Computer Vision*, pages 3523–3532, 2019. 1, 2, 3, 4, 6
- [39] Yue Wang and Justin M Solomon. Prnet: Self-supervised learning for partial-to-partial registration. In *Advances in Neural Information Processing Systems*, pages 8812–8824, 2019. 1, 2, 3, 5, 6
- [40] Y. Wang, Y. Sun, Z. Liu, S. Sarma, M. Bronstein, and J.M. Solomon. Dynamic graph cnn for learning on point clouds. In *ACM Transactions on Graphics (TOG)*, 2019. 2, 4
- [41] Zhirong Wu, Shuran Song, Aditya Khosla, Fisher Yu, Linguang Zhang, Xiaoou Tang, and Jianxiong Xiao. 3d shapenets: A deep representation for volumetric shapes. In *Conference on Computer Vision and Pattern Recognition*, pages 1912–1920, 2015. 5, 7
- [42] H. Yang and L. Carlone. A polynomial-time solution for robust registration with extreme outlier rates. In *Robotics: Science and Systems Conference*, 2019. 2, 3, 6
- [43] H. Yang, J. Shi, and L. Carlone. Teaser: Fast and certifiable point cloud registration. In *arXiv Preprint*, 2020. 1, 2, 3, 5, 6
- [44] Jiaolong Yang, Hongdong Li, Dylan Campbell, and Yunde Jia. Go-icp: A globally optimal solution to 3d icp point-set registration. *TPAMI*, 38(11):2241–2254, 2015. 1, 2
- [45] Zi Jian Yew and Gim Hee Lee. Rpm-net: Robust point matching using learned features. In *Conference on Computer Vision and Pattern Recognition*, 2020. 1, 3, 4, 6
- [46] K. M. Yi, E. Trulls, Y. Ono, V. Lepetit, M. Salzmann, and P. Fua. Learning to find good correspondences. In *Conference on Computer Vision and Pattern Recognition*, 2018. 6
- [47] Manzil Zaheer, Satwik Kottur, Siamak Ravanbakhsh, Barnabas Poczos, Russ R Salakhutdinov, and Alexander J Smola. Deep sets. In *NIPS*, pages 3391–3401, 2017. 2
- [48] Andy Zeng, Shuran Song, Matthias Nießner, Matthew Fisher, Jianxiong Xiao, and Thomas Funkhouser. 3dmatch: Learning local geometric descriptors from rgb-d reconstructions. In *Conference on Computer Vision and Pattern Recognition*, pages 1802–1811, 2017. 2, 6
- [49] Qian-Yi Zhou, Jaesik Park, and Vladlen Koltun. Fast global registration. In *European Conference on Computer Vision*, pages 766–782. Springer, 2016. 1, 2, 6
- [50] Qian-Yi Zhou, Jaesik Park, and Vladlen Koltun. Open3d: A modern library for 3d data processing. In *arXiv Preprint*, 2018. 6